Synthesis and Characterization of $Ba_3Mo_{18}O_{28}$: A Metal–Metal-Bonded Oligomer Containing Four Trans Edge-Shared Molybdenum Octahedra

George L. Schimek, Dick A. Nagaki,† and Robert E. McCarley*

Ames Laboratory, USDOE, and Department of Chemistry, Iowa State University, Ames, Iowa 50011

Received October 6, 1993®

$Ba_3Mo_{18}O_{28}$, a new member in the series $M_{n-x}Mo_{4n+2}O_{6n+4}$, has been synthesized at 1230 °C. Single crystals can be prepared through a transport reaction utilizing $BaMoO_4$, MoO_2, and Mo reagents in the presence of water vapor. Its properties are characterized via single-crystal and powder X-ray diffraction, magnetic susceptibility, and electrical resistivity measurements. $Ba_3Mo_{18}O_{28}$ crystallizes in the centrosymmetric monoclinic space group, $P2_1/a$, with cell parameters a = 9.939(2) Å, b = 9.377(2) Å, c = 13.057(2) Å, β = 100.92(1)°, V = 1194.7(3) Å^3, Z = 2, and R = 0.0427 (R_w = 0.0509) for 1284 reflections with $I > 3\sigma(I)$. The compound contains $Mo_{18}O_{42}$ clusters with strong metal–metal bonding. These clusters consist of four trans edge-shared molybdenum octahedra bridged on all edges by oxygen atoms. A prominent feature of these tetrameric units is the extreme short–long–short arrangement of apical–apical molybdenum bond distances. The tetrameric clusters are interconnected in a stair-step fashion via Mo–O bonding. The sharing of oxygen atoms between clusters can be represented by the connectivity formula $[(Mo_{18}O^{i}_{14}O^{i-i}_{4/2}O^{i-a}_{12/2})O^{a-i}_{12/2}]^{6-}$. Pockets created by the interconnected clusters are filled with barium atoms. Mo–Mo bond order and Mo–O bond valence sums indicate 61.7(6) and 58(2) electrons available for metal–metal bonding (MCE), respectively. The bond valence sums are in excellent agreement with the 58 MCE expected on the basis of formal oxidation states. This compound was found to have a large χ_{TIP} contribution to the magnetic susceptibility. Resistivity measurements on a sintered, pressed pellet showed that the material is a small band gap semiconductor, as expected from the long (>3.17 Å) intercluster Mo–Mo distances.

Introduction

The discovery of $NaMo_4O_6$[1] exposed a whole new field of ternary reduced molybdenum oxide chemistry, materials containing infinite chains of trans edge-shared molybdenum octahedra. One of the goals of the present research has been to "cut" the infinite chains into segments, or oligomers, in order to form new compounds, and thereby determine how the properties of these new materials differ from those of the $M_xMo_4O_6$ phases.[1-9]

These oligomeric compounds can be derived from the general formulation, $M_{n-x}Mo_{4n+2}O_{6n+4}$, where n is equal to the number of edge-sharing Mo octahedra. The value of x is dependent upon the cluster electron count and/or cation coordination preferred. In members of this series with n equal to 1[10] and 2,[3,11-15] x is 0; i.e., the cation pockets are fully occupied. However, when n equals 3,[16,17] x ranges from 0 to about 0.75. In $Ba_3Mo_{18}O_{28}$, n = 4, we have determined that x is 1.

The first compound reported in this oligomeric series, $In_{11}Mo_{40}O_{62}$,[18] contained a 1:1 ratio of Mo_{18} (four edge-sharing octahedra) and Mo_{22} (five edge-sharing octahedra) clusters. High-resolution electron microscopy studies on the indium-containing oligomers indicated that intergrowth regions with four, five, and six trans edge-shared Mo octahedra were possible. However, they did not necessarily grow in an ordered manner. In fact, the structure for the pentameric $In_6Mo_{22}O_{34}$ was reported recently[19] and the authors discussed the difficulty of solving the structure due to intergrowth of oligomers with varying lengths and different modes of stacking. This observation indicates, to some extent, the small differences in thermodynamic stability that must occur among these oligomers and their different stacking modes. With this insight, the difficulty in synthesizing pure oligomers with only one type of cluster and one mode of stacking can be appreciated. The synthesis, structure, and physical properties of $Ba_3Mo_{18}O_{28}$, the first pure n = 4 oligomeric compound, are discussed, and the structural aspects of this compound are compared to those of the Mo_{18} cluster found in $In_{11}Mo_{40}O_{62}$.

Experimental Section

Synthesis. The starting reagents included $BaMoO_4$, MoO_2, and Mo. Barium molybdate was prepared by the metathetical reaction of aqueous solutions of barium chloride dihydrate (Baker Analyzed reagent, 99.6%) and sodium molybdate dihydrate (Fisher Certified). Molybdenum dioxide (Alfa, 99%), molybdenum powder (Aldrich, 99.99%), and the barium molybdate were dried *in vacuo* at 120 °C overnight.

The tetrameric (n = 4) oligomer was first discovered as heavily twinned black, chunklike crystals in a multiphase product obtained from a reaction (1230 °C/7 days) intended to prepare the quaternary monomeric oligomer $LaBaMo_{12}O_{20}$ ($2 \times MMo_6O_{10}$). Subsequent synthetic work showed that good crystals of $Ba_3Mo_{18}O_{28}$ could be synthesized by loading a loose powder containing an intimate mixture of $BaMoO_4$, MoO_2, and Mo in a 3:8:7 mole ratio, with 1.5 mg of $BaCl_2 \cdot 2H_2O$ into a fused silica tube (4–6 cm in length and 5–8 mm in diameter). The evacuated, fused silica ampule was fired at 1230 °C for 15 days. At this reaction temperature, the total vapor pressure resulting from the water of the barium chloride

† Present address: ICD—Catalyst Center, Union Carbide Corp., South Charleston, WV 25303-0361.

• Abstract published in *Advance ACS Abstracts,* March 1, 1994.

(1) Torardi, C. C.; McCarley, R. E. *J. Am. Chem. Soc.* **1979**, *101*, 3963.
(2) Lii, K. H.; Edwards, P. A.; Brough, L. F.; McCarley, R. E. *J. Solid State Chem.* **1985**, *57*, 17.
(3) Torardi, C. C.; McCarley, R. E. *J. Solid State Chem.* **1981**, *37*, 393.
(4) Aufdembrink, B. A. Ph.D. Dissertation, Iowa State University, Ames, IA, 1985.
(5) Torardi, C. C.; McCarley, R. E. *J. Less-Common Met.* **1986**, *116*, 169.
(6) Chen, S. C. Ph.D. Dissertation, Iowa State University, Ames, IA, 1991.
(7) Bauer, K.; Rau, F.; Abriel, W.; Range, K.-J. *Vortragstagung Fachgruppe Festkörperchemie*; Gesellschaft Deutscher Chemiker: Stuttgart, Germany, 1980.
(8) Ramanujachary, K. V.; Greenblatt, M.; Jones, E. B.; McCarroll, W. H. *J. Solid State Chem.* **1993**, *102*, 69.
(9) Simon, A. *Angew. Chem., Int. Ed. Engl.* **1988**, *27*, 160.
(10) Lii, K. H.; Wang C. C.; Wang, S. L. *J. Solid State Chem.* **1988**, *77*, 407.
(11) Hibble, S. J.; Cheetham, A. K.; Bogle, A. R. L.; Wakerley, H. R.; Cox, D. E. *J. Am. Chem. Soc.* **1988**, *110*, 3295.
(12) Dronskowski, R.; Simon, A. *Angew. Chem., Int. Ed. Engl.* **1989**, *28*, 758.
(13) Gougeon, P.; Potel, M.; Sergent, M. *Acta Crystallogr.* **1990**, *C46*, 1188.
(14) Gougeon, P.; Gall, P.; Sergent, M. *Acta Crystallogr.* **1991**, *C47*, 421.
(15) Schimek, G. L.; Chen, S. C.; McCarley, R. E. Manuscript in progress.
(16) Dronskowski, R.; Simon, A. *Acta Chem. Scand.* **1991**, *45*, 850.
(17) Schimek, G. L.; Chen, S. C.; McCarley, R. E. *Inorg. Chem.*, submitted for publication.
(18) Mattausch, Hj.; Simon A.; Peters, E.-M. *Inorg. Chem.* **1986**, *25*, 3428.
(19) Dronskowski, R.; Mattausch, Hj.; Simon, A. *Z. Anorg. Alleg. Chem.* **1993**, *619*, 1397.

0020-1669/94/1333-1259$04.50/0

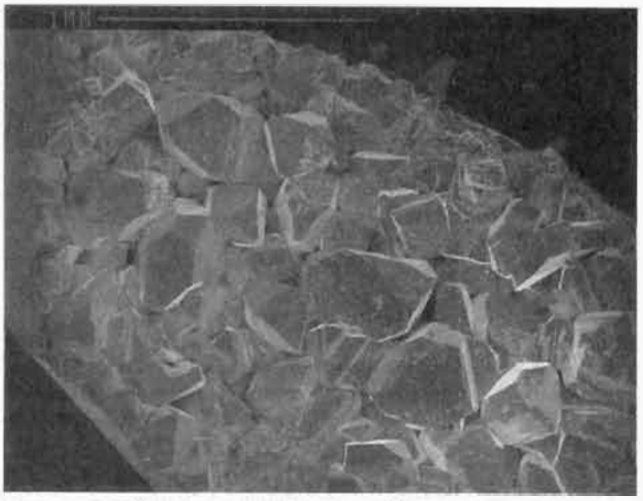

Figure 1. SEM micrograph of transported $Ba_3Mo_{18}O_{28}$ on fused silica. The small fragments on the crystal surfaces are fused silica.

dihydrate was about 1 atm. The reaction mixture was cooled at ~1 °C/min to 1150 °C and ~2 °C/min to 800 °C; then the reaction was quenched to room temperature. In this case, not only were large, chunklike crystals formed by transport, as shown in Figure 1, but some crystals were also found dispersed in the loose, black, bulk powder. Good single-phase, microcrystalline $Ba_3Mo_{18}O_{28}$, on the basis of Guinier powder diffraction patterns, subsequently was prepared in fused silica reaction vessels by omitting the dihydrate salt, using anhydrous reagents, firing the mixture at 1230 °C for 8.5 days, and utilizing the above cooling schedule.

Poor crystal growth of $Ba_3Mo_{18}O_{28}$ was observed when only stoichiometric quantities of $BaMoO_4$, MoO_2, and Mo were utilized. Initially, barium chloride was deemed an essential ingredient for the growth of larger crystals. Reactions including trace to 50 wt % anhydrous barium chloride (mp 963 °C) as a flux were completed. Generally, a larger quantity of barium chloride resulted in more, although badly twinned, crystals that were transported to the cool end of the fused silica tube. Subsequently, it was determined that the $BaCl_2$ was not the necessary component, but, rather, the presence of trace amounts of water, in the form of $BaCl_2{\cdot}2H_2O$. To confirm that water was the transport agent, the same reaction was run with NH_4Cl, instead of $BaCl_2$. In this case, the transported product was MoO_2, thus eliminating the possibility of HCl as the transport agent for this tetrameric oligomer.

X-ray Powder Diffraction. An Enraf-Nonius Delft FR552 triple-focusing Guinier X-ray powder diffraction camera was used with Cu $K\alpha_1$ radiation (λ = 1.540 562 Å). National Institute of Standards and Technology (NIST) silicon powder was used as an external standard. A sample was also analyzed with a Scintag 2000 powder θ–θ diffractometer using Cu $K\alpha_1$ radiation. For the Scintag, the sample was pressed into a recessed region of a single-crystal quartz plate. Lattice parameters derived from a linear least-squares fit of 54 reflections indicated a monoclinic cell with a = 9.940(2) Å, b = 9.355(3) Å, c = 13.112(4) Å, and β = 100.7(1)°.

X-ray Single-Crystal Study. A large, black, chunklike crystal with good faces was indexed and found to be twinned. The crystal was broken, and a fragment having the dimensions 0.04 × 0.07 × 0.10 mm³ was remounted on a glass fiber with Devcon 5-min epoxy resin. As judged from the diffraction data, the crystal quality of this fragment was deemed satisfactory. A Rigaku AFC6R rotating-anode diffractometer, equipped with graphite-monochromated Mo $K\alpha$ radiation (λ = 0.710 69 Å) generated at 7 kW, was used. Lattice parameters and an orientation matrix for data collection were derived from 25 randomly located and centered reflections with a 2θ range of 13–19°. Three standard reflections were measured every 150 reflections and showed no apparent variation in intensity during the data collection. Data were collected at 23 °C from 0 to 50° in 2θ in the hemisphere ($\pm h,+k,\pm l$), using an ω–2θ scan mode. The number of reflections measured was 4587, of which 2599 were unique and 1284 were observed with $I > 3\sigma(I)$. The linear absorption coefficient for Mo $K\alpha$ was 138.45 cm⁻¹. An empirical absorption correction[20] was applied based upon azimuthal scans of three reflections with an average transmission range of 0.763–1.000. The intensity data were also corrected for Lorentz and polarization effects.

Structure Solution and Refinement. The space group $P2_1/a$ (No. 14) was chosen on the basis of the systematic absences of $h0l$ ($h \neq 2n$) and $0k0$: ($k \neq 2n$) with violations for (100), (010), and ($\bar{5}06$), all of which were located near quite intense reflections. The ($30\bar{3}$) reflection was also in violation of the $h0l$ ($h \neq 2n$) condition for the space group $P2_1/a$; however, this reflection could be eliminated because the ($60\bar{6}$) reflection was very intense. This violation most likely arose from $\lambda/2$ radiation. Equivalent data were averaged and resulted in an agreement factor of R_{av} = 4.7%. The structure was solved by direct methods using SHELXS[21] (R = 0.049) and refined on $|F|$ by full-matrix, least-squares techniques[22] with the TEXSAN[23] package. Initial molybdenum atom positions were input on the basis of the SHELXS direct methods output. Subsequent atomic positions for the cation and oxygen atoms were located by Fourier difference maps. These parameters converged at R = 11% when the Ba2 position was allowed to move off the origin and its occupancy varied. Refinement of the isotropic thermal parameters decreased R to 8.0%. The thermal parameters of the cations, seven of the nine molybdenum atoms, and two oxygen atoms were then refined anisotropically and gave R = 5.5%.

A secondary extinction correction was applied and refined to 3.6(2) × 10^{-7}. Although this correction was relatively small, it allowed the thermal parameters of the two remaining isotropically refined Mo atoms and two more oxygen atoms to be refined anisotropically. The barium occupancy and thermal parameters were varied simultaneously for both cations. Ba1 did not deviate from full occupancy and was therefore fixed at that value. The total occupancy of Ba2 was refined to 99.8(2)% over two inversion-related sites, one each located on either side of the origin. A refinement in the lower symmetry space group Pa was performed to examine the possibility that the Ba2 positions were not disordered. This refinement led to R = 0.052 and resulted in three fully occupied Ba positions. However, in Pa a large residual electron density remained at the site occupied by Ba2 in the centric space group. Thus it was considered that the disorder of the Ba2 atoms was real and the refinement in $P2_1/a$ was accepted as superior.

The final refinement in $P2_1/a$ converged at R = 0.0427 and R_w = 0.0509 and had a maximum shift of 0.006 while refining on 182 variables. All molybdenum, barium, and 4 of 14 oxygen atom thermal parameters were refined anisotropically. The temperature factors for the remaining ten oxygen atoms would only refine isotropically, with O12 having an unusually small thermal parameter. A final electron difference map showed that the largest peak of 5.2 e/Å³ was located at the centers of the octahedra found at either end of the n = 4 cluster and the smallest peak of –1.6 e/Å³ was located 0.7 Å from Mo5. Given the relatively large quantity of electron density remaining, the central position was refined as an oxygen (all distances were acceptable Mo–O bond lengths) with varying degrees of population. However, all refinements with this extra atom diverged. This residual electron density and the behavior of the thermal parameters of the oxygen atoms might be the result of the low data to parameter ratio (7:1) or a poor absorption correction but more likely intergrowth of other oligomers or the occurrence of stacking faults. Details of the data collection and refinement for $Ba_3Mo_{18}O_{28}$ are given in Table 1. Final positional parameters and isotropic temperature parameters are given in Table 2.

Magnetic Susceptibility. The magnetic properties were examined on samples of selected crystals with a Quantum Design SQUID magnetosusceptometer. The samples were loaded into a 3 mm inner diameter fused silica tube that had been sealed on the bottom half with 3 mm outer diameter fused silica rod. Another fused silica rod was placed on top of the sample, thus giving an arrangement where a uniform measurement could be made on the sample. The data were subsequently corrected for the diamagnetic contribution of the quartz.

Electrical Resistivity. Electrical resistivity measurements were carried out on a pressed pellet (8800 psi) that had been sintered in an evacuated fused silica ampule at 1230 °C for 12 h after the initial synthesis. This measurement was based on the van der Pauw[24] four-probe method for electrical conductivity.

(20) North, A. C. T.; Phillips, D. C.; Mathews, F. S. *Acta Crystallogr.* **1968**, *A24*, 351.

(21) Sheldrick, G. M. *Crystallographic Computing 3*; Oxford University Press: Oxford, U.K., 1985.

(22) Busing, W. R.; Martin, K. O.; Levy, H. A. ORFLS: A FORTRAN Crystallographic Least Squares Program. Report ORNL-TM-305; Oak Ridge National Laboratory: Oak Ridge, TN, 1962.

(23) *TEXSAN: Single Crystal Structure Analysis Software*, Version 5.0; Molecular Structure Corp.: The Woodlands, TX 77381, 1989.

(24) van der Pauw, L. J. *Phillips Res. Rep.* **1958**, *13*, 1.

Table 1. X-ray Crystallographic Data for $Ba_3Mo_{18}O_{28}$

formula	$Ba_3Mo_{18}O_{28}$
fw	2586.89
crystal system	monoclinic
space group	$P2_1/a$ (No. 14)
a, Å	9.939(2)
b, Å	9.377(2)
c, Å	13.057(2)
β, deg	100.92(1)
V, Å^3	1194.7(3)
Z	2
calcd dens, g/cm^3	7.190
radiation; λ, Å (graphite monochromator)	Mo Kα; 0.710 69
μ(Mo Kα), cm^{-1}	138.45
quality of fit[a]	1.59
R,[b] R_w[c]	0.0427, 0.0509

[a] Quality of fit = $[\sum w(|F_o| - |F_c|)^2/(N_{observns} - N_{params})]^{1/2}$. [b] $R = \sum||F_o| - |F_c||/\sum|F_o|$. [c] $R_w = [\sum w(|F_o| - |F_c|)^2/\sum w|F_o|^2]^{1/2}$; $w = 1/\sigma^2(|F_o|)$.

Table 2. Atomic Coordinates for $Ba_3Mo_{18}O_{28}$

atom[a]	x	y	z	B_{eq},[b] Å^2
Ba1	0.5747(1)	0.5079(2)	0.3434(1)	1.09(5)
Ba2[c]	0.5162(3)	0.4989(3)	0.0627(2)	0.7(1)
Mo1	0.4165(2)	0.1103(2)	0.9989(1)	0.31(6)
Mo2	0.4648(2)	0.1204(2)	0.2151(1)	0.35(6)
Mo3	0.3559(2)	0.1179(2)	0.7823(1)	0.29(6)
Mo4	0.6248(2)	0.1276(2)	0.8783(1)	0.29(6)
Mo5	0.5726(2)	0.1222(2)	0.6756(1)	0.36(7)
Mo6	0.6847(2)	0.1307(2)	0.1211(1)	0.28(6)
Mo7	0.7360(2)	0.1319(2)	0.3229(1)	0.36(6)
Mo8	0.5320(2)	0.1261(2)	0.4270(1)	0.38(6)
Mo9	0.3032(2)	0.1135(2)	0.5710(1)	0.38(7)
O1	0.578(1)	0.249(1)	0.999(1)	0.4(2)
O2	0.753(1)	0.753(1)	0.334(1)	0.6(3)
O3	0.687(1)	0.258(1)	0.443(1)	0.6(3)
O4	0.490(1)	0.735(2)	0.224(1)	0.7(6)
O5	0.411(2)	0.247(2)	0.330(1)	0.7(3)
O6	0.620(1)	0.269(2)	0.220(1)	0.7(6)
O7	0.247(1)	0.482(1)	0.000(1)	0.3(2)
O8	0.352(1)	0.242(2)	0.109(1)	0.7(3)
O9	0.648(1)	0.508(2)	0.560(1)	0.8(5)
O10	0.317(1)	0.498(2)	0.221(1)	0.8(5)
O11	0.793(1)	0.504(2)	0.221(1)	0.5(2)
O12	0.298(1)	0.242(1)	0.888(1)	0.1(2)
O13	0.370(1)	0.996(2)	0.449(1)	0.3(5)
O14	0.536(1)	0.767(1)	0.450(1)	0.4(2)

[a] All atoms reside on the Wyckoff position 4e. [b] The equivalent isotropic temperature factor, B_{eq}, is defined as $(8\pi^2/3)[\sum_i\sum_j(U_{ij}a^*_i a^*_j \vec{a}_i\vec{a}_j)]$, where the summations of i and j range from 1 to 3. [c] Ba2 is split off the special position (2a) $^1/_2$, $^1/_2$, 0; each of the two positions with an occupancy of 49.9(1)%.

Results

Description of Structure. The basic building block of $Ba_3Mo_{18}O_{28}$ is the $Mo_{18}O_{42}$ cluster, consisting of four trans edge-shared molybdenum octahedra bridged on all edges by oxygen atoms and capped by oxygen atoms on the apical Mo atoms. The ORTEP[25] drawing of Figure 2 a illustrates the tetrameric cluster unit. The most notable irregularity of the structure is that the tetrameric unit has a short–long–short arrangement of apical–apical Mo–Mo bond distances. These short apical–apical molybdenum bond distances, 2.599(3) Å for Mo4–Mo5 and 2.587(3) Å for Mo6–Mo7, are in the region typical of strong single bonds and constitute the strongest metal–metal bonds in $Ba_3Mo_{18}O_{28}$. The pairing of the outer apical molybdenum atoms creates a central, long apical–apical distance of 3.113(2) Å for Mo4–Mo6′, which is essentially nonbonding. We note that the basal-plane molybdenum bond angles of 175.7(1)° for Mo8–Mo2–Mo1′, 175.7(1)° for Mo2–Mo1′–Mo3′, and 177.2(1)° for Mo1–Mo3–Mo9 represent little tilting of the adjacent Mo octahedra. Thus the apical–apical pairing interactions do not result from tilting of the octahedra, as is the case for $Sc_{0.75}Zn_{1.25}Mo_4O_7$.[26] The short apical–apical bond distances then result from a displacement of Mo4 and Mo5, or Mo6 and Mo7, toward each other along the long axis of the oligomer. We shall refer to this displacement as the sliding mode of apical–apical bond formation.

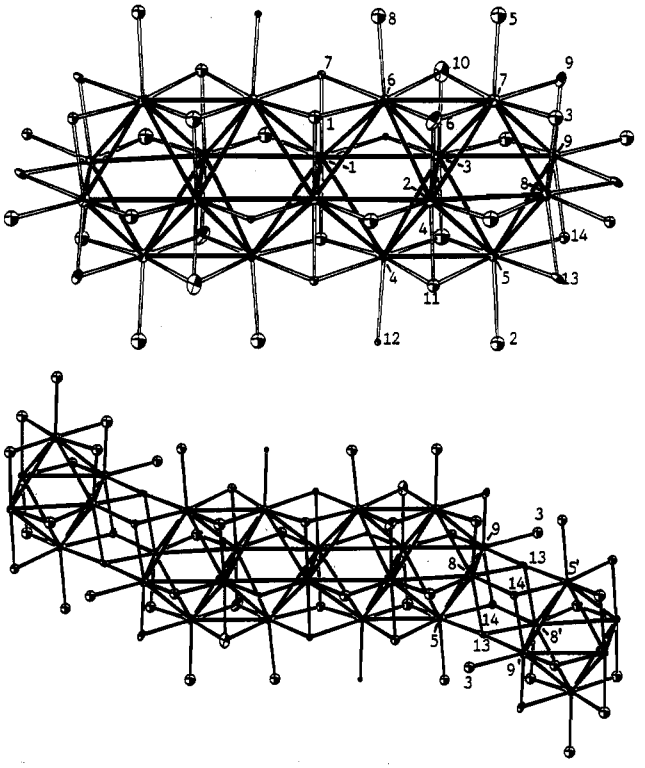

Figure 2. (a) Top: ORTEP drawing of the tetrameric cluster unit, $Mo_{18}O_{42}$, of $Ba_3Mo_{18}O_{28}$ using 70% thermal ellipsoids. Note the short–long–short arrangement of apical–apical molybdenum bonds. (b) Bottom: The tetrameric cluster unit emphasizing Mo–O intercluster connections in a stair-step manner.

The bond distances along the shared edges of the octahedral units follow the opposite trend seen in the apical–apical bond distances. If the apical–apical distance above (and below) the corresponding shared edge is very short, then the Mo–Mo bond distance of that shared edge will be longer than the average shared-edge bond length, and vice versa. In $Ba_3Mo_{18}O_{28}$, the shared-edge (and apical–apical) distances are 2.854(3) Å for Mo2–Mo3 [2.599(3) Å for Mo4–Mo5 and 2.587(3) Å for Mo6–Mo7] and 2.650(4) Å for Mo1–Mo1′ [3.113(2) Å for Mo4–Mo6′]. The Mo–Mo bond distances of the basal edges parallel to the chain direction are arranged in a less dramatic short–long–long–short fashion: 2.720(3) Å for Mo8–Mo2, 2.775(3) Å for Mo1–Mo2′, 2.778(3) Å for Mo1–Mo3, and 2.710(3) Å for Mo3–Mo9. The three shortest intercluster metal–metal distances are 3.176(4) Å for Mo8–Mo8′, 3.195(3) Å for Mo5–Mo8′, and 3.216(3) Å for Mo8–Mo9′. These intercluster distances are rather long for members of this series and are essentially nonbonding. A complete list of metal–metal bond distances is found in Table 3.

Within the Mo_{18} cluster, six molybdenums are only four-coordinate in oxygen (Mo1, Mo2, and Mo3) and the remaining twelve molybdenums are five-coordinate in oxygen (Mo4 to Mo9). The molybdenum–oxygen bond distances vary from 1.90(2) Å for Mo9–O9 to 2.20(1) Å for Mo9–O3′. The average Mo–O bond distance is 2.06 Å. Both of the extreme molybdenum–oxygen distances occur within the region where intercluster bonding couples the tetrameric units together through Mo–O–

(25) Johnson, C. K. ORTEP-II: A FORTRAN Thermal-Ellipsoid Plot Program. Report ORNL-5138; Oak Ridge National Laboratory: Oak Ridge, TN, 1976.

(26) (a) McCarley, R. E. *ACS Symp. Ser.* **1983**, *211*, 273. (b) McCarley, R. E. *Philos. Trans. R. Soc. London, A* **1982**, *308*, 141.

Table 3. Selected Metal–Metal Interatomic Distances (Å) for $Ba_3Mo_{18}O_{28}$[a]

Mo1–Mo1′	2.650(4)	Mo1–Mo2′	2.775(3)
Mo1–Mo3	2.778(3)	Mo1–Mo4	2.833(3)
Mo1′–Mo4	2.822(3)	Mo1–Mo6	2.842(3)
Mo1′–Mo6	2.824(3)	Mo2–Mo3	2.854(3)
Mo2–Mo4	2.697(3)	Mo2–Mo5	2.747(3)
Mo2–Mo6	2.704(3)	Mo2–Mo7	2.796(3)
Mo2–Mo8	2.720(3)	Mo3–Mo4	2.730(3)
Mo3–Mo5	2.778(2)	Mo3–Mo6	2.716(3)
Mo3–Mo7	2.780(3)	Mo3–Mo9	2.710(3)
Mo4–Mo5	2.599(3) ap[b]	Mo4–Mo6′	3.113(2) ap
Mo5–Mo8	2.786(3)	Mo5–Mo8′	3.195(3) inter[c]
Mo5–Mo9	2.767(3)	Mo6–Mo7	2.587(3) ap
Mo7–Mo8	2.646(3)	Mo7–Mo9	2.752(3)
Mo8–Mo8′	3.176(4) inter	Mo8–Mo9	2.777(3)
Mo8–Mo9′	3.216(3) inter	Ba2···Ba2′[d]	1.607(5)
Ba1···Ba2	3.603(3)	Ba1···Ba1′	4.609(3)

[a] Atoms with primed numbers are related to those with unprimed numbers by the inversion center. [b] Apical–apical Mo–Mo bond distances. [c] Intercluster Mo–Mo bond distances. [d] Each barium at 49.9% occupancy.

Table 4. Selected Metal–Oxygen Bond Distances (Å) for $Ba_3Mo_{18}O_{28}$[a]

Mo1–O1	2.06(1)	Mo1–O7′	2.03(1)
Mo1–O8′	2.08(1)	Mo1–O12′	2.09(1)
Mo2–O5′	2.07(2)	Mo2–O6	2.07(1)
Mo2–O8′	1.97(1)	Mo2–O11′	2.08(1)
Mo3–O2′	2.07(1)	Mo3–O4′	2.08(1)
Mo3–O10	2.05(2)	Mo3–O12′	1.97(1)
Mo4–O1′	2.07(1)	Mo4–O4′	2.04(1)
Mo4–O7′	2.08(1)	Mo4–O11′	2.02(1)
Mo4–O12′	2.10(1)	Mo5–O2′	2.15(1)
Mo5–O4′	2.05(1)	Mo5–O11′	2.03(1)
Mo5–O13′	2.13(1)	Mo5–O14′	2.07(1)
Mo6–O1	2.06(1)	Mo6–O6	2.02(1)
Mo6–O7	2.09(1)	Mo6–O8	2.08(1)
Mo6–O10	2.06(1)	Mo7–O3	2.09(1)
Mo7–O5	2.06(1)	Mo7–O6	2.04(1)
Mo7–O9	2.09(2)	Mo7–O10	2.07(2)
Mo8–O3	1.96(1)	Mo8–O5′	1.94(1)
Mo8–O13′	2.08(1) inter[b]	Mo8–O13′	2.07(1)
Mo8–O14′	2.11(1) inter	Mo9–O2′	1.92(1)
Mo9–O3′	2.20(1) inter	Mo9–O9	1.90(2)
Mo9–O13′	2.14(1)	Mo9–O14′	2.02(1)
Ba1–O2	2.92(1)	Ba1–O3	2.81(1)
Ba1–O4	2.68(2)	Ba1–O5	2.93(1)
Ba1–O6	2.85(1)	Ba1–O9′	2.78(1)
Ba1–O9	2.75(1)	Ba1–O10	2.75(1)
Ba1–O11	2.93(1)	Ba1–O13	3.00(1)
Ba1–O14	2.86(1)	Ba2–O1	2.60(1)
Ba2–O1′	2.62(1)	Ba2–O4	3.10(1)
Ba2–O6	3.03(1)	Ba2–O7′	2.65(1)
Ba2–O7	2.64(1)	Ba2–O8	3.04(1)
Ba2–O10	3.12(1)	Ba2–O11	3.12(1)
Ba2–O12	3.05(1)		

[a] Atoms with primed numbers are related to those with unprimed numbers by the inversion center. [b] Intercluster Mo–O bond distances.

Mo bonding parallel to the *c* axis. All metal–oxygen bond distances are given in Table 4.

The stair-step fashion in which the tetrameric units are bonded to each other in the *c* axis direction is shown in Figure 2b. This type of interconnection creates a position in the pocket where cation coordination is irregular, and therefore the barium–oxygen and molybdenum–oxygen bond distances vie for a suitable compromise. The coordination sphere of oxygen atoms around the bariums is shown in Figure 3. The cation located adjacent to the end octahedra in the tetrameric unit, Ba1, is eleven-coordinate in oxygen. The barium–oxygen bond distances range from 2.68(2) Å for Ba1–O4 to 3.00(1) Å for Ba1–O13. The second barium is ten-coordinate in oxygen, and the barium–oxygen bond distances range from 2.60(1) Å for Ba2–O1 to 3.12(1) Å for Ba2–O10 and Ba2–O11. Oxygen atoms O1 and O7 are shared between the statistically occupied Ba2, and oxygen atoms O4, O6, O10, and O11 are shared between Ba1 and Ba2. Ba2 resides on one of two sites at any given time, disordered about the special position at the origin. These two sites are separated by only 1.607(5) Å for Ba2–Ba2′ and thus cannot be occupied simultaneously.

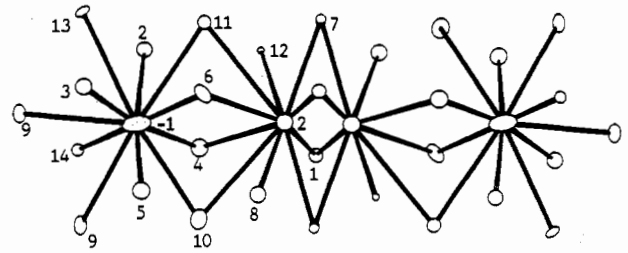

Figure 3. ORTEP drawing (70% thermal ellipsoids) of the coordination environment surrounding bariums in $Ba_3Mo_{18}O_{28}$. Ba2 and Ba2′ are each 50% occupied.

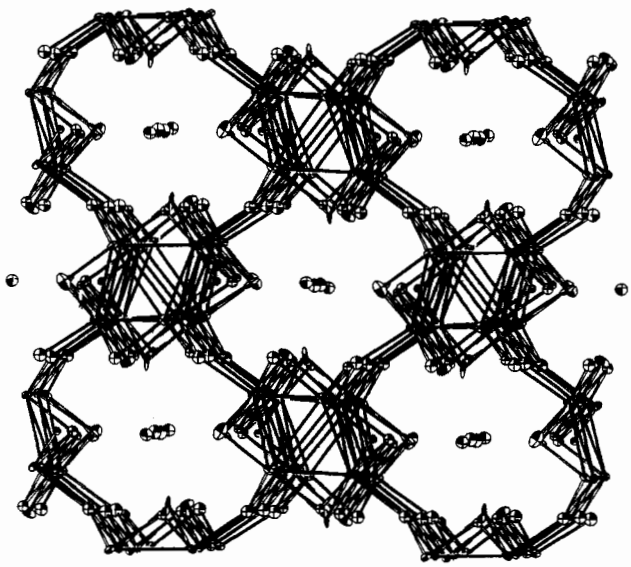

Figure 4. View down the *c* axis of $Ba_3Mo_{18}O_{28}$, parallel to the oligomeric cluster chains, showing the pockets in which the cations reside. Barium–oxygen bonds have been omitted for clarity. Thermal ellipsoids are at 70% probability for this ORTEP drawing.

Figure 4 is an ORTEP drawing of the unit cell of $Ba_3Mo_{18}O_{28}$ as viewed parallel to the *c* axis. From this perspective, the interconnection among Mo_{18} units in the *a* and *b* directions through bridging oxygens can be seen. This cross-linking creates pockets in which the barium cations reside. The view is reminiscent of the infinite-chain compounds, such as $NaMo_4O_6$,[1] and shows that the couplings in the *a*–*b* plane are quite similar.

$Ba_3Mo_{18}O_{28}$ can be described by the following connectivity formula, $Ba^{6+}{}_3[(Mo_{18}O^{i}{}_{14}O^{i-i}{}_{4/2}O^{i-a}{}_{12/2})O^{a-i}{}_{12/2}]^{6-}$. Oxygen atoms O1, O4, O6, O7, O9, O10, and O11 are edge-bridging only within the cluster unit and are labeled O^{i}. The oxygen atoms corresponding to O^{i-i} are edge-sharing between neighboring clusters; these are labelled O13. Oxygens considered O^{i-a} (or O^{a-i}) are edge-bridging between molybdenum atoms of one cluster and terminal to another molybdenum atom in a neighboring cluster (or vice versa); these include O2, O3, O5, O8, O12, and O14.

Discussion

Structural Comparisons. Many similarities exist between the clusters in $Ba_3Mo_{18}O_{28}$ and $In_{11}Mo_{40}O_{62}$.[18] The short–long–short configuration of apical Mo–Mo bond distances was first observed in the $n = 4$ oligomeric cluster of $In_{11}Mo_{40}O_{62}$. The average metal–metal and metal–oxygen bond distances of 2.761 and 2.06 Å, respectively, calculated for the barium end-member are very similar to the 2.789 and 2.07 Å derived in the $n = 4$ cluster of $In_{11}Mo_{40}O_{62}$. The short–long–long–short arrangement of Mo–

Mo bond distances parallel to the chain direction and the pattern of long shared edges when short apical bonds are present (and vice versa) are also observed in the indium member.

The shortest intercluster Mo–Mo bond distances previously determined for oligomers with more than two trans edge-shared Mo octahedra, namely, 2.991(3) Å for $Tl_{1.6}Sn_{1.2}Mo_{14}O_{22}$[16] and greater than 3.20 Å for the mixed oligomer system of $In_{11}Mo_{40}O_{62}$, indicate that there is little, if any, intercluster metal–metal bonding. $Ba_3Mo_{18}O_{28}$ also fits into this pattern.

Cation Considerations. Ba2 probably does not reside at the origin because this situation would require the cation to be in nearly square planar coordination by oxygen. On the Basis of the structural systematics and the general formulation, $M_nMo_{4n+2}O_{6n+4}$, there are four cation sites available, separated on average by the repeat distance between the molybdenum octahedra, ~2.75 Å. This distance would be shorter than twice the ionic radius for Ba^{2+} reported by Shannon.[27] The shortest distances between Ba1 and Ba2, 3.603(3) and 4.609(3) Å for the intercluster Ba1–Ba1′, are more reasonable on the basis of the Shannon ionic radius of 1.52 Å for ten-coordinate Ba^{2+} or 1.57 Å for eleven-coordinate Ba^{2+}. These longer cation–cation separations are expected since $Ba_3Mo_{18}O_{28}$ uses only 75% of the possible cation sites. Cation–cation repulsions are thus relieved by relaxation toward the vacancies.

The statistical occupation of Ba2 raises two questions: (1) Can the cation population be verified by an alternate method? (2) Is there any superstructural ordering due to the partial occupation of barium sites? Confirmation of the composition was carried out by careful electron microprobe analyses of Ba and Mo; oxygen was calculated by difference. Data collected on three different crystals indicated that the composition was $Ba_{3.01(2)}Mo_{18}O_{27.7(1)}$, in excellent agreement with the value determined by crystallographic methods. No superstructure reflections were observed on the basis of the selected area diffraction micrographs taken via transmission electron microscopy. Explicitly, no superstructure parallel to the *c* or *b* axis was detected. Thus Ba2 must be randomly distributed over the two inversion-related sites located near the special position at the origin.

Bond Length–Bond Strength Relationships. The application of bond length–bond strength relationships has provided valuable insights into the structure, bonding, and oxidation states of ternary reduced molybdenum oxides that have been synthesized in this laboratory.[28] The bond order for metal–metal bonds can be determined using Pauling's bond order equation[29] shown in eq 1,

$$d(n) = d(1) - 0.61 \log(n) \qquad (1)$$

where $d(n)$ is the bond distance for a metal–metal bond in question and n is the bond order for that metal–metal bond. $d(1)$ is the metal–metal distance considered as a single bond; for molybdenum this value is 2.614 Å, derived from the distance between nearest and next-nearest neighbors in bcc molybdenum metal. Bond strengths for Mo–O bonds were calculated from the empirical relationship developed by Brown and Wu[30] and given in eq 2. The

$$s(\text{Mo–O}) = [d(\text{Mo–O})/1.882]^{-6.0} \qquad (2)$$

bond strength, in valence units (vu), is given by s(Mo–O), and d(Mo–O) is the observed Mo–O bond distance in angstroms. Since s(Mo–O) is given in valence units, the sum of all Mo–O bond valences about a particular Mo atom will give the valence (oxidation state) of that molybdenum atom.

The numerical values of these calculations are found in Table 5 and reflect the following points. The molybdenum atoms in the interior of the basal plane (Mo1, Mo2, and Mo3) have the highest coordination by other molybdenum atoms and therefore the most electrons available for metal–metal bonding. Apical molybdenum atoms (Mo4, Mo5, Mo6, and Mo7) are five-coordinate in molybdenum (for the observed bonding pattern) and exhibit intermediate metal-centered electron counts. And the molybdenum atoms (Mo8 and Mo9) located at the ends of the cluster unit are four-coordinate in molybdenum (or more depending on intercluster bonding) and have the fewest electrons per molybdenum available for metal–metal bonding.

Table 5. Bond Length–Bond Strength Sums about Mo Atoms of $Ba_3Mo_{18}O_{28}$

atom	Σn(Mo–Mo)	Σs(Mo–O)	$\Sigma n + \Sigma s$
Mo1	3.73(5)	2.30(7)	6.03
Mo2	4.17(5)	2.44(9)	6.61
Mo3	4.04(5)	2.44(7)	6.48
Mo4	3.48(4)	2.90(8)	6.38
Mo5	3.40(4)	2.73(8)	6.13
Mo6	3.53(4)	2.90(8)	6.43
Mo7	3.62(4)	2.83(11)	6.45
Mo8	2.95(3)	3.24(10)	6.19
Mo9	2.49(2)	3.34(13)	5.83

The number of metal-centered electrons (MCE) per $Mo_{18}O_{28}^{6-}$ cluster can be estimated from the sum of the metal–metal bond orders (n) and results in MCE($2\Sigma n$) = 62.8(7) if all bond distances less than 3.22 Å are included or 61.7(6) if the intercluster bond distances are excluded. The total valence of the tetrameric unit based upon the summation of the individual bond valences of the molybdenum atoms derived from Mo–O bonds is $2\Sigma s$ = 50(2) vu. The number of electrons available for metal–metal bonding can also be calculated by subtraction of the 50(2) from 108 (6 × 18), the maximum number of valence electrons available from eighteen molybdenum atoms. The resulting MCE, calculated in this manner, is 58(2). This value is in excellent agreement with the 58 expected on the basis of the formula and the usual formal oxidation states for barium and oxygen.

The MCE value, based on eq 1, of 61.7 electrons is obviously too high, as are the totals including both Σn and Σs, which should not exceed 6.0 for Mo. Evidently the bond orders derived from Pauling's equation are high due to the length used for a Mo–Mo single bond. The value for $d(1)$, 2.614 Å, was derived from the interatomic distances in molybdenum metal. In molybdenum metal, which is body-centered cubic, the environment around each atom is identical. Likewise, each molybdenum atom in the infinite-chain compounds, $M_xMo_4O_6$,[1-9] also has a quite regular environment. Thus, for these materials, this value of $d(1)$ worked well. However, this scenario is not the case for members of the oligomeric series, $M_{n-x}Mo_{4n+2}O_{6n+4}$. Metal–metal bonding of the apical molybdenum atoms and varying degrees of intercluster Mo–Mo bonding in the oligomers create disparate environments, where the coordination number of surrounding metal atoms for any given molybdenum atom is generally lower than that in the infinite-chain compounds. Under such circumstances, a smaller value for $d(1)$ would be appropriate and would lead to smaller bond order sums, as needed here. However, this difficulty of obtaining MCE's that are too high has been found in only one other case, namely $K_3Mo_{14}O_{22}$,[17] where the expected MCE is 43 and that calculated from Pauling bond orders is 45.

The Brown and Wu equation was also utilized to verify the valence of the barium cations. The parameters d(Ba–O) = 2.297 Å and the exponent, –7.0, were employed, and values of 2.56(8) vu for Ba1 and 2.34(5) vu for Ba2 were derived. Both values are above the expected +2; however, similar results were obtained for the n = 1 cluster, $BaMo_6O_{10}$,[10] and n = 2 cluster, $Ba_2Mo_{10}O_{16}$,[6] with calculated valences of 2.6(1) and 2.78(9), respectively.

Magnetic and Resistivity Properties. The magnetic susceptibility of $Ba_3Mo_{18}O_{28}$ was measured on selected crystals over the

(27) Shannon, R. D. *Acta Crystallogr.* **1976**, *A32*, 751.
(28) McCarley, R. E. *Polyhedron* **1986**, *5*, 51.
(29) Pauling, L. *The Nature of the Chemical Bond*, 3rd ed.; Cornell University Press: Ithaca, NY, 1960.
(30) Brown, I. D.; Wu, K. K. *Acta Crystallogr.* **1976**, *B32*, 1957.

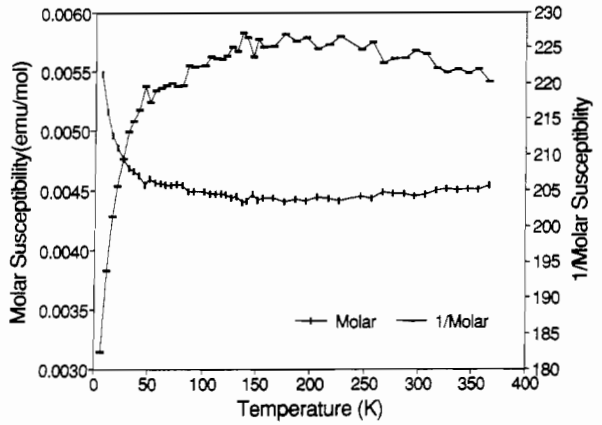

Figure 5. Corrected molar and inverse molar magnetic susceptibility versus temperature for $Ba_3Mo_{18}O_{28}$.

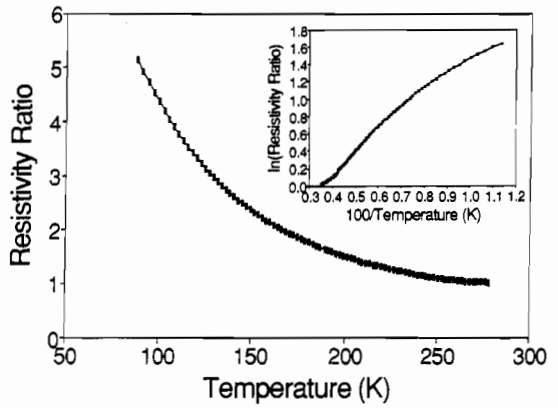

Figure 6. Resistivity ratio of $Ba_3Mo_{18}O_{28}$ plotted versus temperature. The inset shows the nearly linear relationship between the natural logarithm versus 1/T data, indicating semiconducting behavior.

temperature range 6–356 K. The data have been corrected for diamagnetic core contributions based on values reported by Selwood.[31] Figure 5 displays both the molar and inverse molar magnetic susceptibilities for the tetrameric compound. The small tail from 6 to 50 K most likely arises from paramagnetic impurities. Interestingly, the susceptibility levels off at about $\sim 4500 \times 10^{-6}$ emu/mol from 50 to 300 K with a slight increase in the slope above 300 K. This value would imply either that the compound is Pauli paramagnetic or that the cluster has a residual susceptibility (due to temperature-independent paramagnetism, χ_{TIP}) of about 250×10^{-6} emu/Mo, which is large but not unreasonable. The relative flatness of the data above 50 K indicates that the material is essentially devoid of unpaired electrons, in agreement with the calculated even electron count and the expected nondegeneracy of molecular orbital energy levels.

If $Ba_3Mo_{18}O_{28}$ were Pauli paramagnetic, it would imply that the compound should be metallic. For resistivity measurements, attempts to attach leads to large crystals failed, due in part to the chunklike nature in which the crystals grow. Most crystals were no larger than 0.5 mm in the longest dimension. Therefore, a sintered, pressed pellet of the tetramer was subjected to resistivity studies. The sample was measured from liquid-nitrogen (77 K) to room temperature (295 K), as the system slowly warmed with evaporation of the coolant. The resistivity of this sample at 295 K was $\sim 8.8\ \Omega$, or $\sim 2.6\ \Omega$ cm. Plots of the resistivity ratio ($\rho(T)/\rho(295)$) versus temperature and the natural log of the resistivity ratio versus (temperature)$^{-1}$ (inset) are shown in Figure 6. The increasing resistivity with decreasing temperature clearly indicates the semiconducting behavior of $Ba_3Mo_{18}O_{28}$. As can be observed from the inset, the data cannot be linearly fit ($\ln(\rho(T)/\rho(295))$ vs T^{-1}), as would be expected for a strictly semiconducting material. The changing slope would seem to imply a changing size in the band gap, most likely due to impurities in the sample. Nonetheless, the semiconducting behavior excludes the possibility that the material is Pauli paramagnetic.

Electronic Comparisons. The formal removal of one electron from $Mo_{18}O_{28}^{7-}$ in $In_{11}Mo_{40}O_{62}$[18] to $Mo_{18}O_{28}^{6-}$ of $Ba_3Mo_{18}O_{28}$ does not appear to change the structural features markedly. The long, central apical–apical distance is observed in both instances. However, with the above electron change, the short apical–apical distances decrease by about 0.07 Å. In this regard, Wheeler and Hoffmann[32] found that the HOMO–LUMO gap in these Mo_{18} clusters widened as the apical–apical pairing became stronger (shorter Mo4–Mo5 and Mo6–Mo7 distances). Thus, with $Mo_{18}O_{28}^{6-}$, the lower level is filled and the upper level is empty. With $Mo_{18}O_{28}^{7-}$, the upper level (formerly the LUMO) now contains one electron and may be slightly antibonding with respect to these apical–apical interactions. Overall then, the apical–apical bonding should be reduced and the gap between these levels diminished for the higher electron count.

In a more recent paper concerning $In_6Mo_{22}O_{34}$, Simon and co-workers[19] discussed the magnetic and electrical properties of members of the series $M_{n-x}Mo_{4n+2}O_{6n+4}$ with growing oligomer size. According to that assessment, both μ_{eff} and χ_{TIP} increase with increasing n, except for μ_{eff} of $In_6Mo_{22}O_{34}$, which was anomalously low. However, their assessment was made for one specific compound at each n and thus does not account in any way for the effects of different MCE counts at a given n. It is understandable that even- and odd-electron species should exhibit different magnetic properties. But a clear interpretation of measured properties is difficult because of the common occurrence of intergrowth domains containing larger or smaller oligomers in crystals of any given member of the series. Among the different domains for a given n, even the MCE count might be variable. Thus properties obtained by measurements on bulk samples which have not been thoroughly analyzed for compositional and constitutional variations within and among individual crystallites should be interpreted cautiously.

On the basis of the curve presented by Simon and co-workers,[19] $Ba_3Mo_{18}O_{28}$ should have shown a magnetic moment of *ca.* 1.4 μ_B and χ_{TIP} of *ca.* 1740×10^{-6} emu. The observed values are *ca.* 0 μ_B and 4500×10^{-6} emu, respectively. The large discrepancy between the "predicted" and observed properties reflects the difficulties discussed above. As indicated before, the lack of a magnetic moment is understandable in terms of an even-electron system with all spins paired. The origin of the unusually high χ_{TIP} is unknown. It may stem from an unusually close spacing of MO's, giving rise to the van Vleck high-frequency terms, peculiar to this particular cluster species and electron count.

Conclusions

The structural aspects of the pure $n = 4$ oligomeric compound, $Ba_3Mo_{18}O_{28}$, are very similar to those reported by Simon[18] for the analogous cluster in $In_{11}Mo_{40}O_{62}$. Apical–apical molybdenum bond distances follow an extreme short–long–short arrangement, and the average metal–metal and metal–oxygen bond distances are comparable to those of the indium member. As the chain length increases, intercluster Mo–Mo distances become long and the cluster units tend to be interconnected via Mo–O bonds only; such is the case for $Ba_3Mo_{18}O_{28}$. Perhaps the greatest benefit from the analysis of $Ba_3Mo_{18}O_{28}$ can be the certainty that the barium cations are isolated (i.e. no metal–metal bonding) and are in a fixed oxidation state (Ba^{2+}), such that the cluster unit can be considered as a $Mo_{18}O_{28}^{6-}$ unit with definite charge from an electronic point of view. Bond order sums around the

(31) Selwood, P. W. *Magnetochemistry*, 2nd ed.; Interscience Publishers: New York, 1956; p 78.

(32) Wheeler, R. A.; Hoffmann, R. *J. Am. Chem. Soc.* **1988**, *110*, 7315.

molybdenum atoms result in a larger than expected number of MCE, most likely due to the choice of $d(1)$, the length of a molybdenum–molybdenum single bond. The summation of the individual Mo–O bond valences predicts 58(2) electrons available for metal–metal bonding, which coincides with that expected on the basis of known oxidation states for barium and oxygen.

Magnetic susceptibility measurements show that the tetrameric oligomer is electron-paired but does have a substantial temperature-independent paramagnetic susceptibility. The lack of unpaired electrons is in agreement with the even electron count and a relatively large HOMO–LUMO energy gap predicted by Wheeler and Hoffmann[32] for the case where apical–apical Mo distances show paired distortions. Pressed-pellet resistivity measurements confirm that the material is not Pauli paramagnetic but is actually a small band gap semiconductor.

Acknowledgment. We thank Dr. Robert A. Jacobson for many insightful crystallographic discussions. Assistance with the magnetic susceptibility and resistivity measurements was provided by Jerry Ostenson and Zhaorong Wang, respectively. The microprobe analyses were completed by Dr. Alfred Kracher, Department of Geological and Atmospheric Sciences, Iowa State University. This work was supported by the U.S. Department of Energy, Office of Basic Energy Sciences, through Ames Laboratory operated by Iowa State University under Contract No. W-7405-Eng-82.

Supplementary Material Available: Tables listing data collection details, anisotropic thermal parameters, and bond angle information (3 pages). Ordering information is given on any current masthead page.